Title

Detecting resting-state brain activity by spontaneous cerebral blood volume fluctuations using whole brain vascular space occupancy imaging

Authors

Miao, Xinyuan
Gu, Hong
Yan, Lirong
et al.

Publication Date

2014

DOI

10.1016/j.neuroimage.2013.09.019

Peer reviewed

NeuroImage 84 (2014) 575–584

Contents lists available at ScienceDirect

NeuroImage

journal homepage: www.elsevier.com/locate/ynimg

Detecting resting-state brain activity by spontaneous cerebral blood volume fluctuations using whole brain vascular space occupancy imaging

Xinyuan Miao [a,b,c], Hong Gu [d], Lirong Yan [c,e], Hanzhang Lu [f], Danny J.J. Wang [c,e], Xiaohong Joe Zhou [g], Yan Zhuo [a,c,*], Yihong Yang [d,**]

[a] State Key Laboratory of Brain and Cognitive Science, Beijing MRI Center for Brain Research, Institute of Biophysics, Chinese Academy of Sciences, Beijing, China
[b] University of Chinese Academy of Sciences, Beijing, China
[c] UCLA–Beijing Joint Center for Advanced Brain Imaging, Beijing, China; Los Angeles, CA, USA
[d] Neuroimaging Research Branch, National Institute on Drug Abuse, National Institutes of Health, Baltimore, MD, USA
[e] Department of Neurology, UCLA, Los Angeles, CA, USA
[f] University of Texas Southwestern Medical Center, Dallas, TX, USA
[g] Center for Magnetic Resonance Research and Department of Radiology, Center for Magnetic Resonance Research, University of Illinois at Chicago, Chicago, IL, USA

ARTICLE INFO

Article history:
Accepted 12 September 2013
Available online 20 September 2013

Keywords:
Resting-state fMRI
Brain networks
Cerebral blood volume
VASO
BOLD

ABSTRACT

Resting-state brain activity has been investigated extensively using BOLD contrast. However, BOLD signal represents the combined effects of multiple physiological processes and its spatial localization is less accurate than that of cerebral blood flow and volume (CBF and CBF, respectively). In this study, we demonstrate that resting-state brain activity can be reliably detected by spontaneous fluctuations of CBV-weighted signal using whole-brain gradient and spin echo (GRASE) based vascular space occupancy (VASO) imaging. Specifically, using independent component analysis, intrinsic brain networks, including default mode, salience, executive control, visual, auditory, and sensorimotor networks were revealed robustly by the VASO technique. We further demonstrate that task-evoked VASO signal aligned well with expected gray matter areas, while blood-oxygenation level dependent (BOLD) signal extended outside of these areas probably due to their different spatial specificity. The improved spatial localization of VASO is consistent with previous studies using animal models. Moreover, we showed that the 3D-GRASE VASO images had reduced susceptibility-induced signal voiding, compared to the BOLD technique. This is attributed to the fact that VASO does not require T_2^* weighting, thus the acquisition can use a shorter TE and can employ spin-echo scheme. Consequently VASO-based functional connectivity signals were well preserved in brain regions that tend to suffer from signal loss and geometric distortion in BOLD, such as orbital prefrontal cortex. Our study suggests that 3D-GRASE VASO imaging, with its improved spatial specificity and less sensitivity to susceptibility artifacts, may have advantages in resting-state fMRI studies.

Published by Elsevier Inc.

Introduction

There has been growing interest in intrinsic brain activities revealed by spontaneous fluctuations in resting-state functional MRI (rs-fMRI) signals (Biswal et al., 1995; Fox et al., 2005; Greicius et al., 2003). The human brain has been shown to be composed of multiple coherent networks that support sensory, motor and cognitive functions (Buzsáki and Draguhn, 2004; De Luca et al., 2006; Smith et al., 2009). These brain networks appear to be consistent across time within and between individuals (Chen et al., 2008; Damoiseaux et al., 2006), and constrained to anatomically connected regions (Greicius et al., 2009; Honey et al., 2009). Interestingly, the strength of functional connectivity in these networks at "rest" is able to predict relevant task-induced activation and behavioral performance (Hampson et al., 2006; Zou et al., in press). Alterations of resting-state activity in these brain networks are associated with various neurological and psychiatric disorders (Buckner et al., 2008; Menon, 2011), suggesting that intrinsic brain activities may be used as a system-level biomarker for diagnosing diseases and monitoring treatment outcomes.

Although intrinsic brain activity can be assessed using various modalities, including electrophysiology (Arieli et al., 1996; Fiser et al., 2004), positron emission tomography (Raichle et al., 2001) and voltage-sensitive dye imaging (Mohajerani et al., 2010), the majority of current knowledge about it has been acquired from resting-state blood-oxygenation level dependent (BOLD) imaging studies (Biswal et al.,

* Correspondence to: Y. Zhuo, State Key Laboratory of Brain and Cognitive Science, Beijing MRI Center for Brain Research, Institute of Biophysics, Chinese Academy of Sciences, Beijing 100101, China.
** Correspondence to: Y. Yang, Neuroimaging Research Branch, National Institute on Drug Abuse, National Institutes of Health, Baltimore, MD 21224, USA.
E-mail addresses: yzhuo@bcslab.ibp.ac.cn (Y. Zhuo), yihongyang@intra.nida.nih.gov (Y. Yang).

1053-8119/$ – see front matter. Published by Elsevier Inc.
http://dx.doi.org/10.1016/j.neuroimage.2013.09.019

1995; Fox et al., 2005), which constitute a growing proportion of functional brain imaging literature over the past years. However, BOLD signal represents the combined effects of cerebral blood volume (CBV), cerebral blood flow (CBF) and cerebral metabolic rate of oxygen ($CMRO_2$) (Davis et al., 1998), which may be difficult to interpret without knowing the complex interplay of these physiological parameters. Therefore, imaging techniques based on a less confounding (ideally single), well-interpretable physiological parameter (such as CBV, CBF or $CMRO_2$) are needed. Recently, arterial spin-labeling (ASL) perfusion imaging has been used to investigate resting-state brain activities (Chuang et al., 2008; Viviani et al., 2011; Zou et al., 2009), demonstrating the viability of characterizing intrinsic brain activities with CBF contrast, though low temporal resolution, low contrast-to-noise ratio, and contamination of BOLD signal remain challenging in these techniques. Like CBF, CBV could be another important, single physiological parameter to characterize brain activities with improved spatial specificity (Jin and Kim, 2008), but so far, there is no CBV-based resting-state fMRI study reported in humans yet.

Vascular space occupancy (VASO) imaging was originally proposed to measure task-induced brain activation based on CBV changes from the baseline to an activated state (Donahue et al., 2009; Hua et al., 2013; Lu et al., 2003; Wu et al., 2007; Yang et al., 2005). Evoked fMRI experiments on cat brains showed that VASO signal was primarily located in the middle layers of the cortex (closer to neural cells), whereas BOLD signal based on a gradient-echo sequence was more on the surface layer (closer to blood vessels) (Jin and Kim, 2008), suggesting that VASO has better spatial localization than BOLD. Compared to ASL techniques, which usually need a pair of images to obtain CBF, a single-shot VASO imaging may provide higher temporal resolution.

Theoretically, VASO imaging can be used to measure intrinsic brain activities reflected by fluctuations of CBV, but practically it was limited to only a few brain slices if traditional multi-slice echo-planner imaging (EPI) sequences are used. This is due to the fact that VASO exploits an inversion recovery pulse sequence to acquire images at a limited time duration (blood nulling time) when blood signal is suppressed. However, three-dimensional gradient- and spin-echo (3D-GRASE) VASO sequence (Günther et al., 2005; Poser and Norris, 2009) acquires images in a 3D fashion, and therefore data from the entire brain can be collected at the blood nulling time, implying the possibility of observing changes of CBV in the entire brain.

In this study, we seek to detect resting-state brain activities by spontaneous CBV fluctuations, using 3D-GRASE VASO imaging. Specifically, intrinsic brain networks, including cognitive control, visual, and sensorimotor networks were assessed using a single-shot, whole-brain VASO technique. The CBV-based resting-state brain networks were subsequently compared with the BOLD-based ones obtained from the same participants.

Methods

Subjects and fMRI paradigms

Eighteen healthy subjects (9 males; mean age 22.8 ± 1.8 years) were scanned with normal or correct-to-normal vision after providing written informed consent. Foam pads were used to restrain head motions and scanner noise was attenuated by earplugs. Two resting scans (with VASO and BOLD contrasts respectively) were acquired followed by two task scans (VASO and BOLD respectively), so that the resting-state scans would not suffer from the potential 'footprints' of task performance. The order of VASO and BOLD scans was pseudo-randomized among participants. The subjects were instructed to close their eyes and not to fall in sleep during the resting scans. In the task scans, a block-design visual task with dark-gray and light-gray checkerboard flashing at 8 Hz was used, which began with a 30-s "off" block (with a fixation cross at the center of the screen) and consisted of twelve cycles of alternated 20-s "on" and 20-s "off" blocks. The subjects were asked to tap their fingers simultaneously while viewing the visual stimuli.

VASO and BOLD data acquisition

Experiments were performed on a Siemens 3 T TIM Trio scanner (Siemens, Erlangen, Germany) using the body coil for transmission and a 12-channel head coil for reception. VASO data were acquired using a single-shot 3D GRASE sequence with a non-selective adiabatic inversion pulse, followed by an inversion time (TI) to null the blood signal (Poser and Norris, 2009). Gradients compensating the imbalance in Maxwell terms due to the EPI readout were not used in this GRASE implementation. The body coil-transmitted inversion pulse nulls the blood in a relatively large volume (within an FOV of about 40 cm) and thus reduces inflow effects in the VASO signal. After a spectral-selective saturation pulse for fat suppression, the imaging volume was excited by a slab-selective 90° sinc RF pulse with 5.12 ms duration, subsequently refocused by a 180° sinc pulse that was surrounded by crusher gradients on the z-axis. During each spin echo, an entire k_x–k_y plane was acquired using an EPI readout. Centric order encoding along k_z-direction was used to minimize TE effects and maximize SNR. To avoid blurring due to T_2 decay during the long readout train that was required for a large number of slices, parallel imaging capability was added to allow undersampling in primary (k_y) phase-encoding direction, as well as partial Fourier acquisition along the secondary (k_z) phase-encoding direction.

The acquisition parameters of the VASO sequence were: matrix size $64 \times 64 \times 22$ with 2 additional slices for oversampling, FOV = $220 \times 220 \times 110$ mm^3, voxel size = $3.4 \times 3.4 \times 5$ mm^3, TR/TE/TI = 2500/14.6/742 ms, GRAPPA factor along $k_y = 3$, partial Fourier along $k_z = 6/8$, readout bandwidth = 2694 Hz/pixel, and total readout length = 280 ms. The total acquisition time for both resting and task scan was 8 min and 30 s. TI was determined based on the blood T_1 of 1627 ms (Lu et al., 2004; Poser and Norris, 2011). A gradient-echo EPI sequence was used for BOLD imaging acquisition. For comparison, most acquisition parameters of the BOLD were the same as those of VASO, except for TE (30 ms) and GRAPPA factor (no parallel imaging was used). Finally, a conventional 3D MP-RAGE sequence of 6-min was performed to acquire T_1-weighted images which were used as anatomic reference (voxel size = 1 mm^3 isotropic, TI = 1100 ms, TR = 2530 ms, flip angle = 7°, $256 \times 256 \times 176$, GRAPPA factor = 2).

Task-based fMRI data analyses

The task-based VASO and BOLD data were preprocessed using Matlab (The MathWorks, Inc., MA, USA) and SPM8 (http://www.fil.ion.ucl.ac.uk/spm/), which included slice timing correction (only for BOLD data), image realignment, coregistration of structural and functional data, and normalization to the MNI space. Spatial smoothing with a 6-mm full-width-at-half-maximum (FWHM) Gaussian kernel along x and y directions was applied to VASO data, while the BOLD data were smoothed with a 3-D 6-mm Gaussian kernel. There was no large head motion observed (>2 mm), and all data were included in the following analysis.

The hemodynamic response function (HRF) of VASO signals (with inverted sign) may differ slightly from that of BOLD (Lu et al., 2003). However, in this study we adopted a block-design paradigm, which would be insensitive to the minor differences in the hemodynamic responses of VASO and BOLD signals, and thus the same HRF by default in SPM was used for the both contrasts. Since VASO signal decreases in activated condition, first-level statistical analysis defined the 'on's as −1 and 'off's as 0 for VASO-based task data, and 'on's as 1 and 'off's as 0 for BOLD-based ones. The timing of block conditions took into account inversion time in VASO. A group-level statistics was then performed to obtain the activation maps for VASO and BOLD contrasts, respectively. Average VASO and BOLD percentage changes were calculated in a region

of interest (ROI) within the visual cortex, defined by the intersection of the respective group activation maps and the masks of Brodmann area 17 (http://fmri.wfubmc.edu/software/PickAtlas). In this way, the activated voxels were confined to the primary visual cortex and the ROIs of VASO and BOLD were presumed to have similar sizes, so that the fractional signal changes would be contributed primarily from the primary visual cortex and would not be biased dramatically by different numbers of voxels due to different contrast-to-noise ratios (CNR) of the two techniques. The fractional signal changes of the visual ROIs were calculated as:

$$\frac{\Delta S_i}{S_{0,i}} = \frac{S_{a,i} - S_{0,i}}{S_{0,i}} = \frac{\beta_{a,i}}{\beta_{0,i}} \times 100\% \qquad i \in \{\text{VASO, BOLD}\}, \tag{1}$$

where $S_{a,i} = \beta_{a,i} p(t) + \beta_{0,i} + \varepsilon$ and $p(t)$ is the paradigm for the visual task.

Resting-state fMRI data analyses

The resting-state VASO and BOLD data were preprocessed using AFNI (Cox, 1996) with the following steps: slice-timing correction (applied to BOLD data only), motion correction, spatial normalization to the standard Talairach space, quadratic detrending, spatial smoothing, and mean-based intensity normalization of all volumes by the same multiplicative factor. As with the task data, Gaussian spatial smoothing was applied to the VASO resting data along x and y directions only (FWHM = 6 mm), while the BOLD resting data were smoothed along all three directions.

To identify resting functional networks, group independent component analysis (gICA) was applied to both VASO and BOLD resting fMRI data, using the MELODIC tool in the FSL (FMRIB Software Library), an implementation of probabilistic ICA (Beckmann and Smith, 2004). The preprocessed resting data from all 18 subjects were concatenated in the temporal dimension to form a single data set to be fed into the probabilistic ICA algorithm. The number of components was set at 30. All ICA spatial maps were converted to z statistic maps via a normalized mixture-model fit (Beckmann and Smith, 2004) and thresholded at Z > 3.0. The resting functional networks were visually identified based on the similarities to known brain networks (Beckmann et al., 2005).

Seed-based functional connectivity analyses were also performed on the resting-state VASO data for comparison with the gICA generated component maps. In addition to the preprocessing steps used for the gICA analysis, preprocessing for seed-based connectivity analysis included temporal band-pass filtering in the range of 0.01–0.1 Hz and regression of certain nuisance covariates, including time courses of six motion parameters and the first three principal component sets, each calculated based on the time course ensemble from the white matter and the cerebrospinal fluid (CSF) voxels separately (Gu et al., 2010). To generate corresponding network maps, eight seed ROIs were defined in left precentral gyrus (Talairach coordinates: −53, −7, 29), left transverse temporal gyrus (−50, −21, 11), left cuneus (BA 17: −6, −76, 11), left inferior occipital gyrus (BA17: −20, −94, −8), left posterior cingulate cortex (−12, −54, 10), left dorsal cingulate cortex (−4, 26, 34), left inferior parietal cortex (−48, −63, 38), and right inferior parietal cortex (45, −58, 42) (see Fig. S1 in the Supplementary material for the seed ROI definition). Average time course of each seed ROI was extracted as a reference time course to calculate the cross-correlation coefficient (cc) map for each individual. The cc maps were then transformed to z-value maps using Fisher's z transform before entering the group analysis. A one-sample t-test was performed on the z-value maps to obtain significant functional connectivity maps at a group level, which were thresholded at $t_{(17)} > 3.2$ with a cluster size resulting in corrected p-value ($p_{corrected}$) < 0.05 based on Monte Carlo simulations.

Susceptibility effects

The gradient-echo (GE) EPI sequence used in BOLD acquisition is sensitive to susceptibility artifacts at the interfaces of brain tissue and air/bone, which may cause spatial distortion and signal loss, especially in the orbitofrontal cortex (OFC). The 3D-GRASE VASO sequence is intrinsically spin echo weighted with shorter TE, rather than T_2^* weighted, so it is expected to suffer less of susceptibility signal voiding than GE-EPI (Fernández-Seara et al., 2005). To demonstrate different susceptibility effects on the 3D-GRASE VASO and GE-EPI BOLD signals, we investigated the functional connectivity of superior ventral striatum (VSs), which is known to have connections to the OFC (Di Martino et al., 2008), using a seed-based method.

The VSs seed ROI was defined as the head of caudate (HCau) in left hemisphere by the Harvard–Oxford probabilistic atlas (Desikan et al., 2006) in the Talairach space. Based on the atlas, a mask covering the left HCau regions was generated at 50-percent probability. The group functional connectivity maps were thresholded at $t_{(17)} > 5.38$ with a cluster size resulting in corrected p-value ($p_{corrected}$) < 0.05 based on Monte Carlo simulations.

Potential BOLD contribution in VASO signal

To examine explicitly the extravascular BOLD effects in the VASO signal, we conducted an additional experiment on nine healthy subjects (6 males, mean age 24.7 ± 1.93 years). Data of resting-state and task conditions were collected using the 3D-GRASE VASO sequence and a similar sequence without the inversion pulse but keeping all other parameters unchanged. The preprocessing and analysis of the task data were the same as that of the main experiment task data from 18 subjects. The group activation maps were thresholded at $t_{(8)} > 5.7$.

To investigate the potential BOLD effects in resting VASO data, auditory network was delineated using the seed-based method with the same seed region located in the transverse temporal gyrus as used in the analysis of the main experiment resting data. The preprocessing were the same as that of the main experiment resting data as well. The group auditory network maps were thresholded at $t_{(8)} > 5.0$.

Results

Task-induced brain activation

Brain activation induced by the visual stimuli along with finger-tapping from the VASO and BOLD imaging are shown in Figs. 1(a) and (b) (p < 0.001, FDR corrected, t > 4.95). At the same FDR-corrected threshold, the activated areas in the VASO maps were primarily within gray matter, while the activated areas in the BOLD maps were much extensive, probably due to its strong intra- and extra-vascular BOLD effects (Ogawa et al., 1990). Since the higher CNR in BOLD may lead to the spread of BOLD signals, we raised the thresholds of VASO and BOLD t-maps to 7.35 and 7.40, respectively, to maintain an equal number of activated voxels (41,000 mm^3) for both maps (Figs. 1(c) and (d)). Under such condition, the BOLD signals still extended outside of the gray matter areas. These results demonstrated the better spatial specificity of VASO contrast than that of BOLD, which is in agreement with the previous observations in the animal model (Jin and Kim, 2008).

Figs. 1(e) and (f) illustrate the average time courses of VASO and BOLD signals in the activated visual cortex, respectively. The visual ROIs were defined by intersecting the activation maps ($p_{FDRcorrected} < 0.001$, t > 4.95) with the Brodmann area 17, and the volumes were 4392 mm^3 and 3968 mm^3 for VASO and BOLD, respectively. The mean VASO and BOLD signal changes of the 18 subjects were −1.22 ± 0.44% and 2.39 ± 0.81%, respectively, which were within reasonable ranges. These results of task-based fMRI study demonstrate the feasibility of the 3D-GRASE VASO sequence in detecting brain activation and were the foundation of the following resting-state studies.

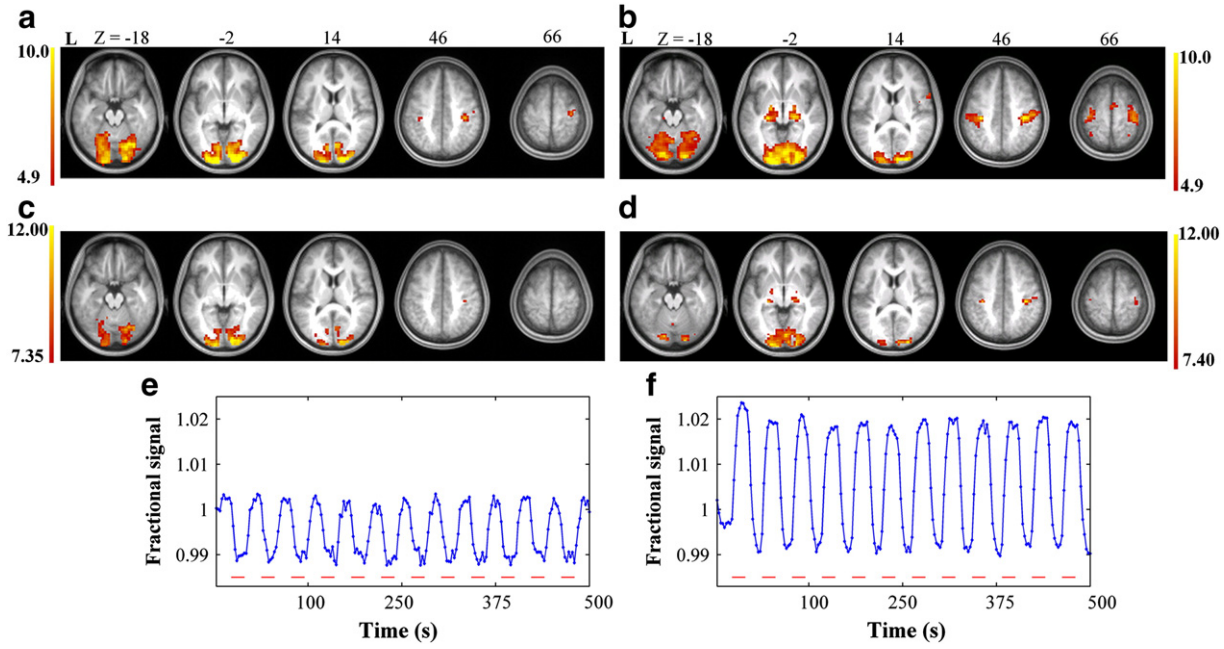

Fig. 1. Task-evoked brain activation maps ($p_{FDR\ corrected} < 0.001$) from VASO (a) and BOLD (b). The threshold was increased for the VASO (c) and BOLD (d) activation maps, such that their activated voxels were almost the same. Average time courses of VASO (e) and BOLD (f) in the activated primary visual cortex, with the red bar presenting stimuli 'on' conditions.

In addition, we found that BOLD fMRI, but not VASO fMRI, detected activation in thalamus and supplementary motor area (SMA), which may reflect the higher sensitivity for BOLD contrast. When we lowered the threshold of VASO t-map ($p < 0.01$, uncorrected, $t < 2.6$) (see Fig. S2 in Supplementary materials), the activation in the thalamus and SMA showed up, although the sensitivity in the thalamus and SMA seemed to be lower than the visual cortex, implying that the lower CNR of VASO signal could lead to false-negative detection of weak activation in areas of thalamus and SMA.

Resting-state brain networks

Of the 30 components generated by gICA on the VASO resting data, eight meaningful resting functional networks were identified based on similarity to previous published results (Beckmann et al., 2005), which included sensorimotor network, auditory network, primary visual network, higher visual network, default-mode network, salience network, left executive-control network (ECN), and right ECN, as shown in Fig. 2(a). For comparison, corresponding functional networks generated from the BOLD resting data were displayed side by side in Fig. 2(b). Spatial cross-correlation between the VASO- and BOLD-based functional networks revealed a high degree of similarity (mean correlation of 0.45). The thresholded VASO-based functional network maps are summarized as follows: *Sensorimotor network* covered bilateral precentral gyrus, bilateral medial frontal gyrus (BA 6), and left culmen. *Auditory network* included bilateral Heschl's gyrus, bilateral superior temporal gyrus, bilateral insula (BA 13), and bilateral dorsal anterior cingulate cortex (BA 24). *Primary visual network* encompassed bilateral calcarine fissure (BA 17), bilateral lingual gyrus (BA 18), and bilateral cuneus. *Higher visual network* covered non-primary regions of visual cortex, including bilateral occipital pole extending laterally towards the occipito-temporal junction (BA 19). *Default-mode network* covered bilateral posterior cingulate, bilateral precuneus, bilateral medial prefrontal cortex/rostral anterior cingulate (BA 9/10), bilateral inferior parietal lobule (BA39), and bilateral middle temporal gyrus (BA 21). *Salience network* encompassed brain regions in bilateral anterior cingulate, bilateral anterior insula, bilateral dorsal lateral prefrontal cortex (DLPFC), right posterior cingulate gyrus (BA 23/31), and bilateral supramarginal gyrus (BA 40). The ECN was decomposed into two strongly lateralized components, which was commonly seen in the BOLD-based resting functional network studies using ICA (Smith et al., 2009). The *left* ECN and *right* ECN covered bilateral DLPFC (BA 9/46), bilateral parietal cortices, bilateral superior temporal gyrus, and left middle temporal gyrus.

The seed-based analysis of the VASO resting data produced similar network maps (Fig. 2(c)), as those from gICA. Differences exist in the network maps between the seed and gICA methods. For example, the gICA-generated ECN has two strong lateralized components while the seed-based ECN maps showed connection to the contralateral side of frontal and parietal regions in addition to the ipsilateral connection. The gICA produced two clean and separate primary visual and higher visual networks, while the corresponding two networks generated by the seed-based methods both extended into the regions belong to the other network.

Susceptibility effects

Due to different image acquisition strategies, VASO and BOLD raw images exhibited very different susceptibility effects in the neighboring areas of air/tissue interfaces, as seen in Fig. 3. GE-EPI based BOLD images showed extensive signal voiding in the inferior frontal regions and the inferior temporal regions, especially in medial OFC, while little susceptibility-induced signal voiding was found in the 3D-GRASE based VASO images.

Different susceptibility effects in VASO and BOLD images were further revealed in the functional connectivity maps of superior ventral striatum (HCau) shown in Fig. 4. To demonstrate the effects of susceptibility-induced signal loss on generating the resting functional connectivity maps and to display the anatomical regions that the left HCau was connected to, the connectivity maps of VASO and BOLD were overlaid on their respective raw images and the high-resolution anatomical images. The VASO- and BOLD-based connectivity maps of left HCau were similar and both maps showed connections to medial OFC/ACC. Despite that, there were two major differences between VASO- and BOLD-based VSs maps in Fig. 4. In the inferior part of the medial OFC (marked by a green arrow) that suffered severe susceptibility-induced signal voiding, BOLD-based connectivity maps showed little/no connectivity to the HCau at the same thresholding level, while VASO-based maps still exhibited connections. The VASO-based VSs connectivity maps

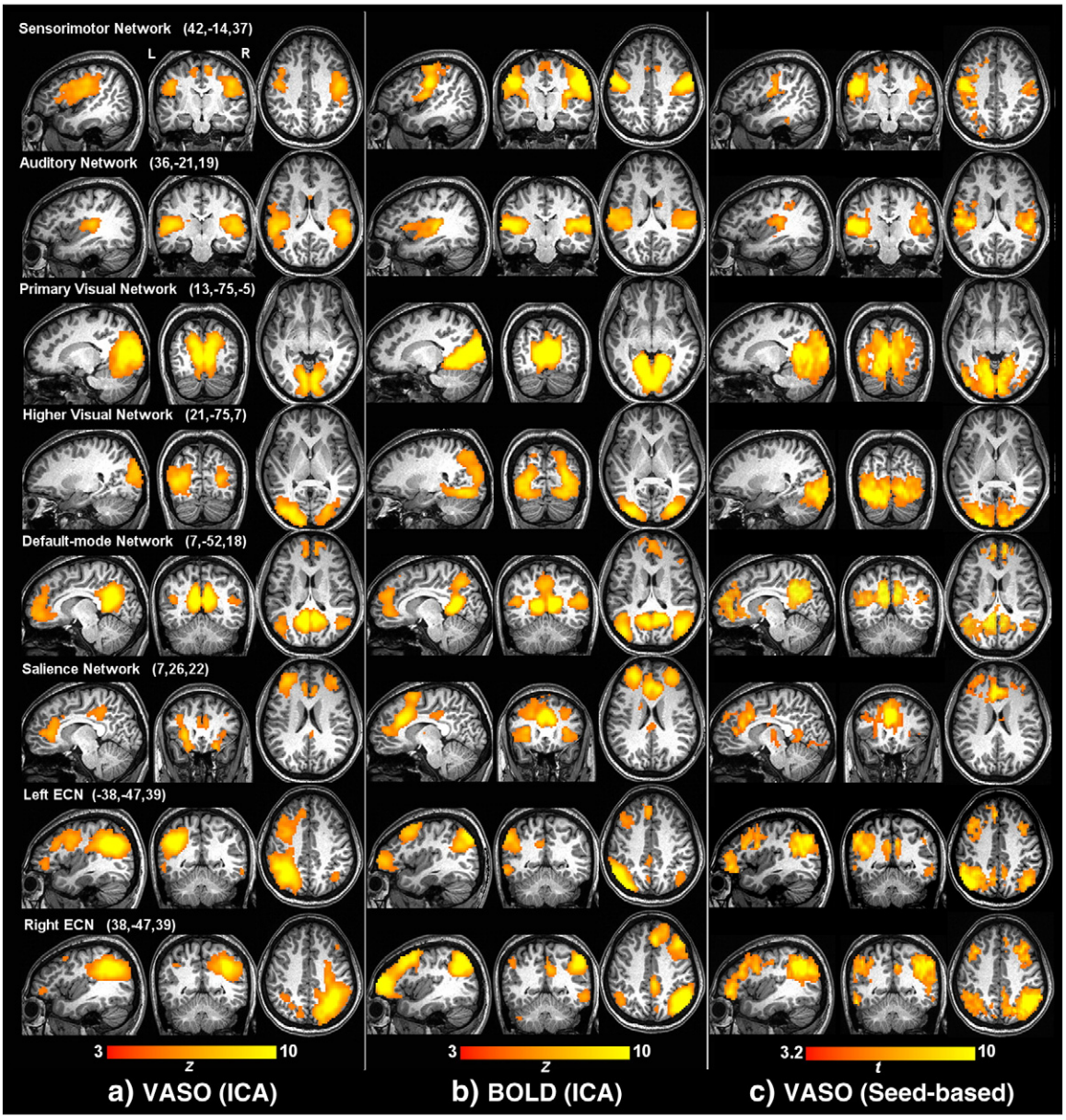

Fig. 2. Brain networks detected by independent component analysis of the VASO (a) and BOLD (b) data, including sensorimotor, auditory, primary visual, higher visual, default mode, salience and executive control networks. The corresponding networks detected by the seed-based analysis of the VASO data were displayed in column (c).

covered parahippocampal gyrus/hippocampus (marked by a green arrow), while BOLD-based connectivity maps of VSs showed no connection to this region, where signals were affected by the susceptibility-induced magnetic field inhomogeneity.

Potential BOLD contribution in VASO signal

Two data sets were acquired using the 3D-GRASE VASO sequence and a similar sequence but without the inversion pulse. The group-level activation t-maps of the two data sets are shown in Figs. 5(a) and (b). To calculate visual stimuli induced signal percentage change, the same visual ROI used in the analysis of the main experimental data was used. The fractional signal changes were $-1.50 \pm 0.57\%$ and $0.35 \pm 0.22\%$ for the VASO and "3D-GRASE without inversion pulse" data, respectively (Fig. 5(c)). The task-induced signal changes of both data sets for each individual were listed in Table S1 in the Supplementary materials. Since both the intra- and extravascular signals contributed to BOLD effects and the intravascular signal was nulled in the VASO data, the extravascular BOLD effects were estimated to contribute about 14% to the VASO signal changes, after taking into account that the extravascular fractions of BOLD signals were approximately 67% at 3 T (Lu and van Zijl, 2005).

With the seed placed in left transverse temporal gyrus, the group auditory network maps were obtained from the two resting data sets (Figs. 6(a) and (b)). It can be seen that the GRASE VASO data showed connectivity with the contralateral side. On the other hand, when GRASE sequence without inversion pulse was used, the data did not manifest any contralateral connectivity, again suggesting that the BOLD effect in the GRASE sequence was small. Note that the strong ipsilateral and local connectivity at short echo times ($\leq$14 ms) has been shown previously and is thought to be due to S_0 contribution rather than true functional connection mediated by T_2^* effect (Wu et al., 2012). The unthresholded z-value map from a single subject and the low-thresholded group auditory network maps from the two resting data sets were displayed in Figs. S3 and S4 as Supplementary materials. The voxel-wise results were confirmed by the ROI results. The

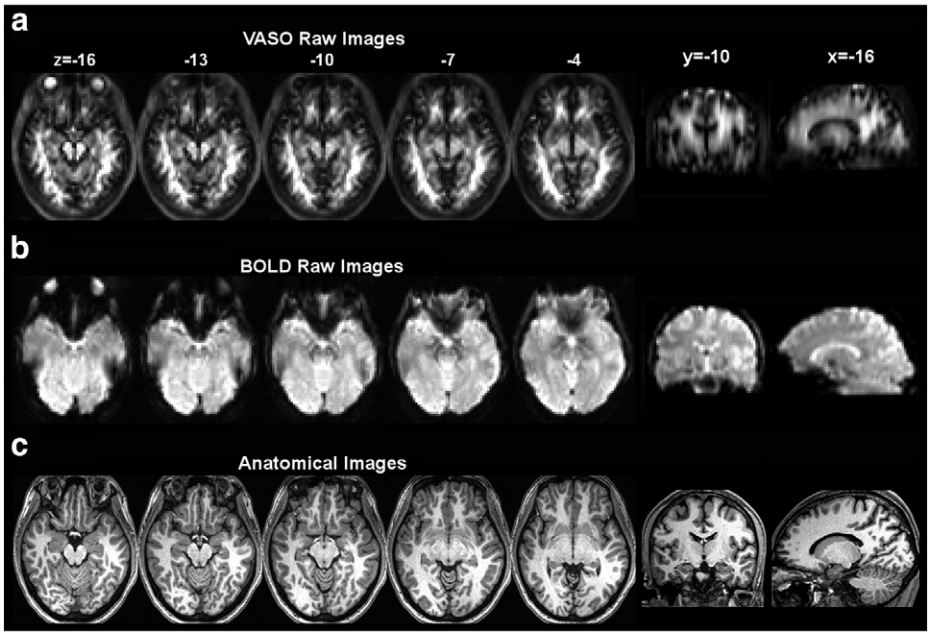

Fig. 3. Raw images of 3D-GRASE VASO (a) and GE-EPI BOLD (b), as well as T_1-weighted anatomical images (c), in the same slices of the inferior brain.

functional connectivity strength in the right auditory cortex (contralateral to the seed region) (assessed by average z-value in the right auditory ROI defined by the main experiment resting data) were 0.18 ± 0.07 for the VASO and −0.03 ± 0.19 for the "3D-GRASE without inversion pulse" data, respectively; the corresponding connectivity strength in the left auditory cortex (ipsilateral to the seed region) were 0.31 ± 0.08 and 0.64 ± 0.07 respectively (Fig. 6(c)). The mean z-value on the contralateral side for the "3D-GRASE without inversion pulse" data was not significantly different from zero ($p = 0.6$), confirming lack of long-range functional connections; while the high mean z-value on the ipsilateral side are thought to be contributed majorly from connectivity-irrelevant S_0 signal (Wu et al., 2012). Individual data were listed in Table S2 in the Supplementary materials. Therefore, similar to the task data, the BOLD effects in the resting data using a GRASE sequence appear to be considerably lower than the CBV effects, although the exact fraction could not be determined due to the small amplitude of this effect.

Discussion

Functional brain connectivity has shown promise in exploring large-scale brain networks and their interactions, and thus providing new insights into system-level understanding of brain functioning (Bressler and Menon, 2010). BOLD imaging has been widely used in resting-state fMRI studies probably due to its high sensitivity and ease for implementation. However, BOLD signal depends on multiple physiological processes (Davis et al., 1998) and therefore is not straightforward to interpret. Furthermore, BOLD signal has relatively poor spatial localization, compared to CBV- and CBF-based signals (Duong et al., 2001; Jin and Kim, 2008). As such, imaging methods based on a less-confounding physiological parameter, such as CBV or CBF, are needed to overcome the drawbacks of BOLD.

In the present study, we used a 3D-GRASE VASO sequence to accomplish whole-brain acquisition of CBV signals in a temporal resolution

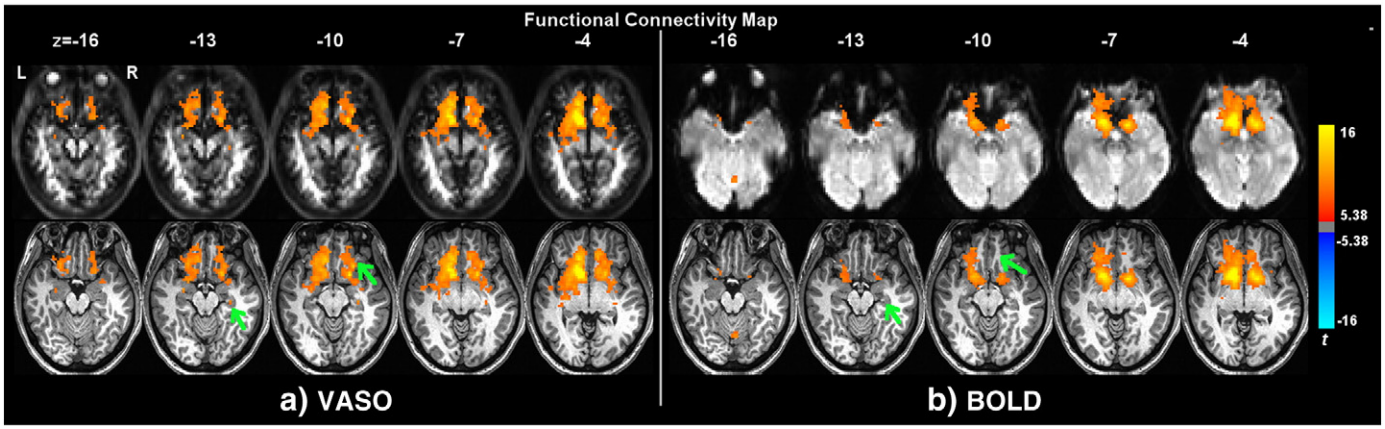

Fig. 4. Functional connectivity maps from the VASO (a) and BOLD (b), using left superior ventral striatum as a seed. The upper row shows functional connectivity maps overlaid on their own raw images (VASO or BOLD), while the bottom row shows the functional connectivity maps overlaid on corresponding anatomical images. The green arrows are pointing at medial OFC and parahippocampal gyrus/hippocampus.

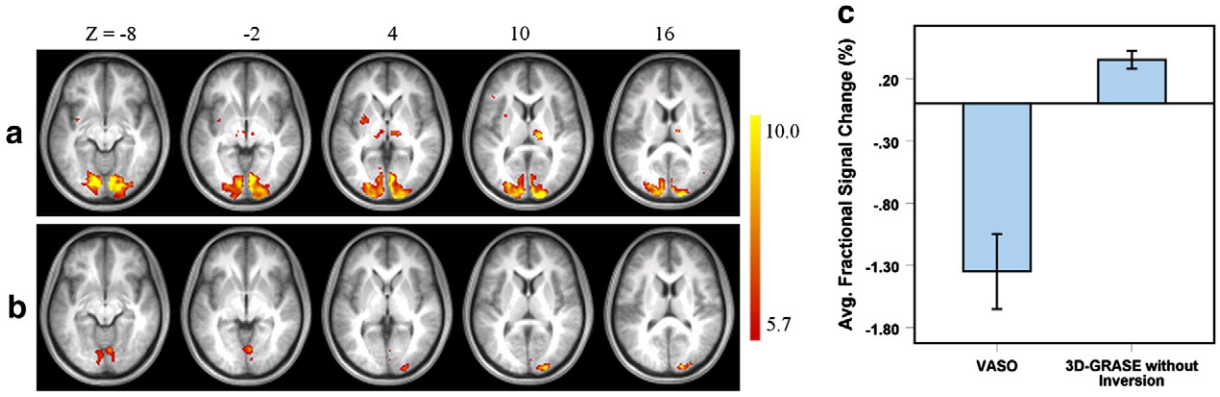

Fig. 5. BOLD effects in the 3D-GRASE VASO sequence assessed from a separate experiment: evidence from the visual task data. Activation maps obtained from the data sets acquired with (a) the 3D-GRASE-VASO sequence and (b) 3D-GRASE sequence without inversion pulse. Bar plot in (c) showed the corresponding average fractional signal changes in the visual ROI defined by the main experiment task data of 18 subjects.

comparable to BOLD methods. Spatial specificity of VASO signal was illustrated in the task fMRI study, in which activation maps from VASO tended to align with gray matter, while activation maps from BOLD spread to outside gray matter. Furthermore, unlike ASL, VASO is not based on an exchange phenomenon and therefore does not rely on the hypothesis of steady-state of the system. As such, it is intrinsically better suited to fMRI than ASL, for which transients between activation and resting epochs do not provide much reliable information.

In the resting-state fMRI study, VASO images acquired in less than 9 min were utilized to detect brain networks. Independent component analysis of the VASO data revealed prominent brain networks including DMN, SN, ECN, visual, auditory and sensorimotor networks, which were largely similar to those obtained using BOLD. Not surprisingly, discrepancies between the network patterns obtained from the BOLD and VASO were also present, especially in the SN and ECN. Although ECN was decomposed into two lateralized components in both VASO and BOLD maps, regions in the BOLD maps seemed more localized to the frontal and parietal areas. Cognitive networks such as SN and ECN are usually less stable in ICA (e.g. ECN could appear as unilateral or bilateral) compared to sensory networks and DMN, suggesting that high sensitivity is needed to detect these cognitive networks robustly. The differences in network patterns between the VASO and BOLD might owe to the different sensitivity and specificity of the two fMRI techniques, but remain to be verified, for example, using animal models (Jin and Kim, 2008).

BOLD functional connectivity analyses are based on dynamic imbalances in CBF/$CMRO_2$, whereas an ability to detect brain networks from CBV fluctuations may raise a concern of potential non-neuronal contributions (e.g., vascular origin) in the resting-state fMRI data. For example, vascular tone exhibits low-frequency oscillations in the absence of stimulus, known as vasomotion (Aalkjær et al., 2011; Hudetz et al., 1998), although the phenomenon is still poorly understood. However, CBV-based resting-state fMRI with a superparamagnetic contrast agent has been performed on a rat model (Lu et al., 2007). The resting-state fMRI signal in the primary somatosensory cortex of the rats correlated with the power coherence of electrophysiological recordings in a region-specific and anesthetic dose-dependent fashion, indicating a neuronal origin of the CBV-weighted signal. In the present study, the brain networks obtained from the VASO imaging showed large-scale spatial distributions (not just local or laterally symmetrical), similar to those of BOLD, suggesting that the signal origin of VASO is similar to that of BOLD.

Image artifacts in gradient-echo EPI, such as signal voiding and geometric distortion caused by magnetic susceptibility differences between brain tissue and air/bone, preclude the assessment of several important brain regions including OFC. Compared to GE-EPI BOLD, the 3D-GRASE sequence used for VASO is less sensitive to the susceptibility-induced signal voiding since it combines gradient and spin echoes in the image acquisition. As demonstrated in this study (Fig. 4), signal voiding in the OFC was severe in the gradient-echo EPI, whereas it was much minor in the 3D-GRASE. As a result, functional connectivity between

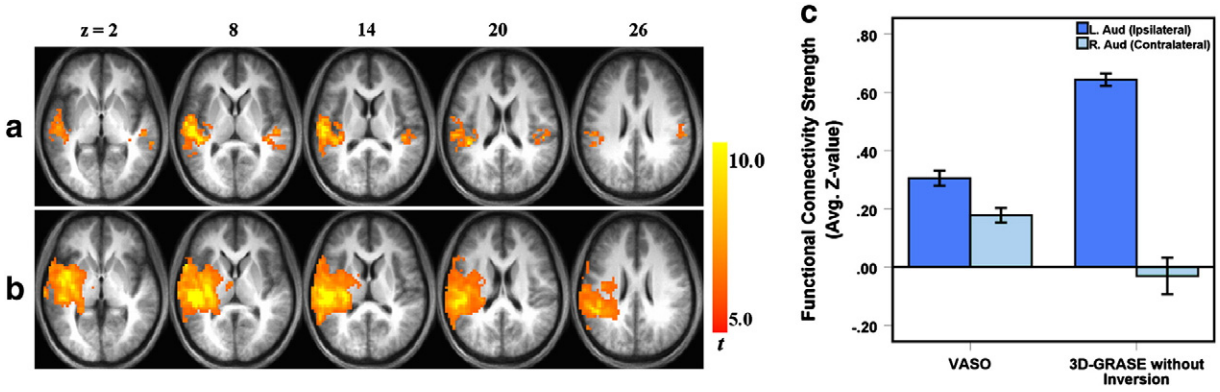

Fig. 6. BOLD effects in the 3D-GRASE VASO sequence assessed from a separate experiment: evidence from the resting data. Group auditory network maps obtained from the data sets acquired with (a) the 3D-GRASE-VASO sequence and (b) 3D-GRASE sequence without inversion pulse with left transverse temporal gyrus (−50, −21, 11) as the seed region ($p < 0.001$, $t_{(8)} > 5.0$). Bar plot in (c) showed the functional connectivity strength to the seed region (assessed by the average z-value) in the left and right auditory ROI defined by the auditory network map from the main experiment resting data of 18 subjects.

the striatum and OFC was detected robustly in the 3D-GRASE VASO but not the gradient-echo EPI BOLD (Fig. 5). This is an important advantage of the 3D-GRASE VASO method, particularly in neuropsychiatric studies in which the OFC and medial temporal lobe are often critical but suffered from susceptibility signal voiding in traditional EPI.

The fractional signal changes ($-1.22 \pm 0.44\%$ in VASO versus $2.39 \pm 0.81\%$ in BOLD) of the task fMRI data were in reasonable ranges, suggesting that the potential confounds of inflow effects and extravascular BOLD contamination were well controlled in the 3D-GRASE VASO sequence. To examine more explicitly the extravascular BOLD effects in the VASO signal, we collected additional data of resting-state and task conditions using the 3D-GRASE VASO sequence and a similar sequence without the inversion pulse. The extravascular BOLD effects were estimated to contribute about 14% to the VASO signal changes. The results of this experiment indicated that CBV-weighted signal dominated in our 3D-GRASE VASO data, while a small amount of BOLD contribution existed, which could be further reduced by shortening TE (e.g. using a larger number of parallel imaging acceleration factor with an RF coil of more channels), but should be cautious when interpreting the data.

The hemodynamic responses of VASO and BOLD seemed to be different (Figs. 1(e) and (f)). The BOLD activation had lasting undershoot in the 20 s "off" interval, while the VASO signal already returned to the baseline. To assess the potential influence of the hemodynamic response function (HRF) selection on the analysis of VASO data, we adjusted the HRF for VASO to diminish its undershoot, as shown in Fig. S5(a) in the Supplementary materials. The adjusted HRF was closer to the empirically obtained VASO signal, and was expected to be more favorable than the SPM default HRF, normally used in the analysis of BOLD data (Fig. S5(b)), for analyzing VASO signals. The VASO data of the 18 participants were reanalyzed using the adjusted HRF, and the generated activation t-maps ($p_{FDR\ corrected} < 0.001$) were shown in Fig. S5(c). For comparison, the group activation maps produced by SPM default HRF, as shown in Fig. 1(a), were also displayed side by side in Fig. S5(d). The spatial distributions of the two activation maps

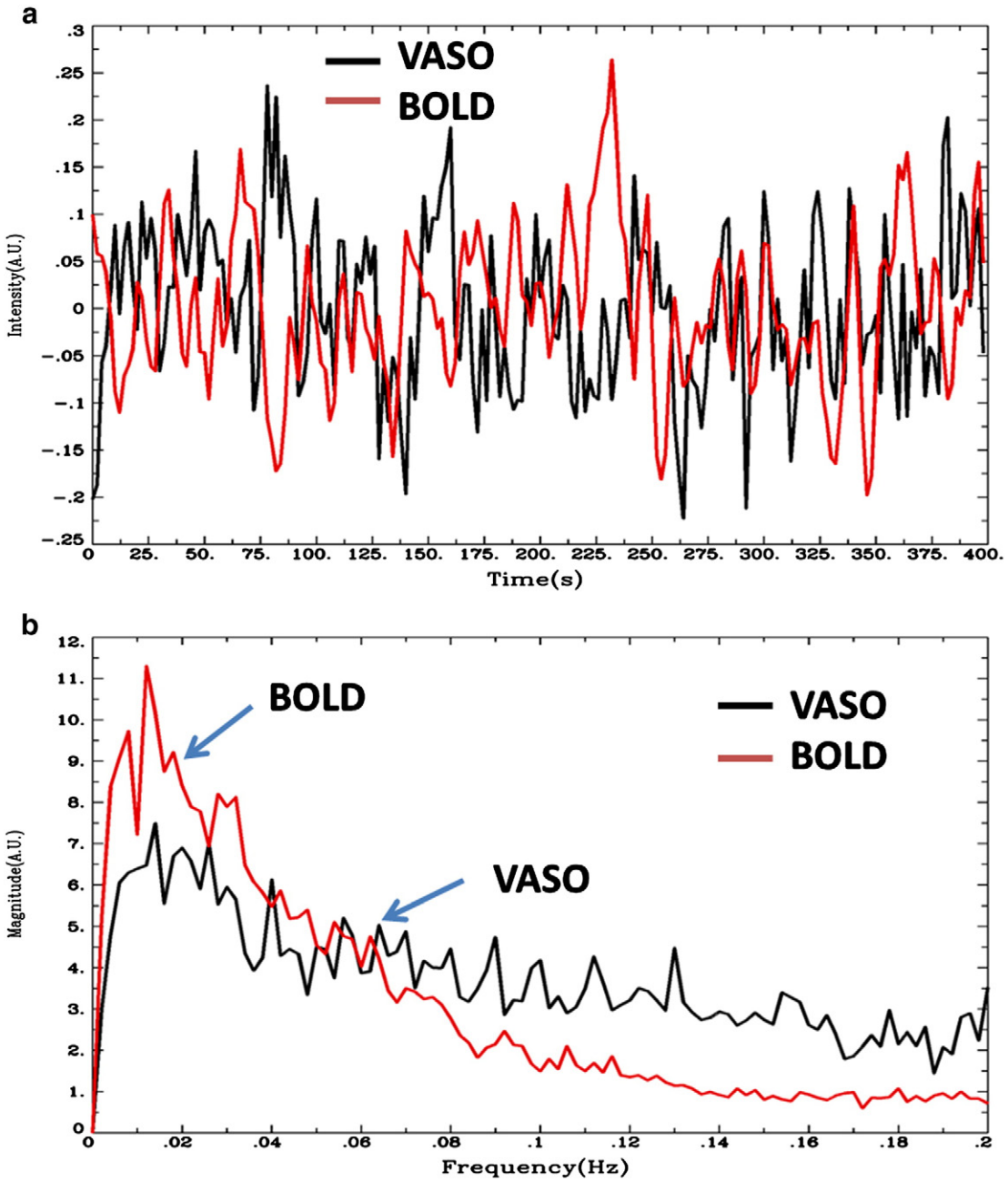

Fig. 7. (a) Mean time courses of VASO and BOLD signals in the primary visual cortex averaged across 18 subjects and (b) their corresponding spectra.

were almost the same for the two HRFs, and the signal change in the visual ROI of the adjusted HRF was $-1.23 \pm 0.45\%$, compared with that with the default HRF of $-1.22 \pm 0.44\%$. The differences were virtually negligible.

The intrinsic temporal fluctuations of the VASO and BOLD signals may be affected by different VASO and BOLD hemodynamic response as well. To inspect the temporal and frequency characteristics of these two contrasts, we extracted unfiltered resting-state VASO and BOLD time courses from the primary visual cortex (defined by the gICA-generated primary visual network) and computed their spectra. Fig. 7 showed the time courses and spectra averaged across all 18 subjects. VASO and BOLD signals seemed to have different temporal and frequency characteristics. The VASO time course shows more high-frequency oscillations, while the fluctuations in BOLD appears to be more low frequency. This can also be seen in the spectra of VASO and BOLD data, in which the magnitude of BOLD spectrum decays faster than that of VASO. While these characteristics seemed interesting, the underlying mechanisms are unknown and their implications in detecting resting-state brain activity needs to be further investigated.

A main limitation of the present study is that VASO signal may contain flow contributions when using a short TR of 2.5 s. Specifically, at the TR used in the present study, the steady-state and equilibrium nulling times differ by more than 400 ms, thus the blood magnetization at the time of image acquisition may depend on its spin history and how many inversion pulses it has experienced prior to RF excitation. In our calculation of spin magnetization, we assumed that the 90° 3D excitation pulse in the previous TR can reset all longitudinal magnetization to 0, and the recovery and inversion times were based on this assumption. While this assumption may be valid for blood that is already inside the 3D imaging slab at the time of the previous excitation, blood spins that arrive at the brain after this time will have a non-zero magnetization. Since these spins will only experience one inversion pulse (the one in the current TR), they are likely to have a negative magnetization, over-estimating the CBV effect. A recent study suggested that, since these newly arrived spins are most likely located in large arterial vessels, their contributions can be minimized by adding crusher gradients equivalent to a cutoff velocity of 3 cm/s (Hua et al., 2013). The present study did not apply crusher gradients as they may disrupt the CPMG condition in the 3D GRASE readout. Thus, we could only calculate the potential vessel-suppressing effect of existing gradient components intrinsic to a 3D GRASE readout. For the head-foot direction which is the typical flow orientation of arterial vessels, the equivalent cutoff velocity in the 3D GRASE readout was found to be 10.6 cm/s, which is greater than the value used in Hua et al. (2013). Since the velocity of blood in human arteries (1–4 mm in diameter) is about 30–50 cm/s, and in arterioles (20–30 μm in diameter) about 2–20 cm/s (B. and N., 1998; Berne and Levy, 1988), we expected that there is still residual flow effect from arterioles in our VASO signal. Thus, the initial findings from the present study require future verifications using a longer TR or using a different CBV method (e.g. nanoparticle contrast agent based).

Another limitation of the 3D-GRASE VASO sequence might be the image blurring, especially in the z-direction, associated with the T_2 decay caused by the long echo train. However, the parallel imaging and partial Fourier acquisition used in this study shortened the echo train length of the 3D-GRASE sequence to 280 ms, which was comparable to that of Poser and Norris (2009). The FWHM of our 3D-GRASE point spread function (PSF) in the z-direction was 1.5 voxels, calculated by Fourier transform of the modulation transfer function (MTF). The MTF of signals was simulated under the approximately same readout condition as the experiment, assuming brain tissue T_1 and T_2 values of 1300 and 100 ms, respectively. The simulated PSF of single-shot 3D-GRASE sequence was comparable to that of a previous study (Vidorreta et al., 2012). Since 3D-GRASE VASO contains additional image blurring in the z-direction during image acquisition, it is desirable to minimize or avoid spatial smoothing along this direction during the post-processing, compared to the BOLD data.

In addition, the influence of CSF signals on VASO signal could partly account for the noise in VASO images, although it could be nulled by another inversion pulse besides the blood nulling one (VASO-FLAIR). However, CSF was shown to contribute more at long TRs (Donahue et al., 2009), which was not likely to be a concern in this study. Moreover, the 3D-GRASE VASO sequence can be further improved by using Maxwell gradient compensation to remove potential image artifacts (Poser and Norris, 2009).

Conclusion

We have demonstrated in the present study that intrinsic brain activity can be assessed by synchronized spontaneous CBV-weighted fluctuations using a 3D-GRASE VASO imaging technique. Reliable brain networks were detected from the CBV-based whole-brain images, including DMN, SN, ECN, visual, auditory and sensorimotor networks. Improved spatial localization of the VASO technique, compared to BOLD, was shown in the task-evoked brain activation, in which activation aligned well with gray matter in VASO but extend to other areas in BOLD. Susceptibility artifacts in the OFC were substantially alleviated in the 3D-GRASE VASO, compared to the gradient-echo EPI BOLD. Functional connectivity between striatum and OFC was detected robustly by the VASO but not the BOLD, indicating advantages of the VASO technique in the assessment of brain regions that are suffered from susceptibility artifacts. These results suggest that 3D-GRASE VASO imaging may become an attractive technique for assessing brain functions in regions that precluded by traditional BOLD techniques.

Acknowledgments

We are grateful to Dr. Matthias Gunther for providing a GRASE sequence. This work was supported in part by the Ministry of Science and Technology of China grant (2012CB825500), the National Nature Science Foundation of China grants (91132302, 90820307, 30830101), the Intramural Research Program of the National Institute on Drug Abuse (NIDA), and R01 NS067015/NS/NINDS NIH HHS/United States.

Appendix A. Supplementary data

Supplementary data to this article can be found online at http://dx.doi.org/10.1016/j.neuroimage.2013.09.019.

References

Aalkjær, C., Boedtkjer, D., Matchkov, V., 2011. Vasomotion — what is currently thought? Acta Physiol. (Oxf.) 202, 253–269.
Arieli, A., Sterkin, A., Grinvald, A., Aertsen, A., 1996. Dynamics of ongoing activity: explanation of the large variability in evoked cortical responses. Science 273, 1868–1871.
B. B.R., N. L.M., 1998. Physiology, In: The C. V. Mosby Company (Ed.), 2nd ed.
Beckmann, C.F., Smith, S.M., 2004. Probabilistic independent component analysis for functional magnetic resonance imaging. IEEE Trans. Med. Imaging 23, 137–152.
Beckmann, C.F., DeLuca, M., Devlin, J.T., Smith, S.M., 2005. Investigations into resting-state connectivity using independent component analysis. Philos. Trans. R. Soc. Lond. B Biol. Sci. 360, 1001–1013.
Berne, R.B., Levy, M.N., 1988. Physiology, In: The C. V. Mosby Company (Ed.), 2nd ed.
Biswal, B., Yetkin, F.Z., Haughton, V.M., Hyde, J.S., 1995. Functional connectivity in the motor cortex of resting human brain using echo-planar MRI. Magn. Reson. Med. 34, 537–541.
Bressler, S.L., Menon, V., 2010. Large-scale brain networks in cognition: emerging methods and principles. Trends Cogn. Sci. 14, 277–290.
Buckner, R.L., Andrews-Hanna, J.R., Schacter, D.L., 2008. The brain's default network: anatomy, function, and relevance to disease. Ann. N. Y. Acad. Sci. 1124, 1–38.
Buzsáki, G., Draguhn, A., 2004. Neuronal oscillations in cortical networks. Science 304, 1926–1929.
Chen, S., Ross, T.J., Zhan, W., Myers, C.S., Chuang, K.S., Heishman, S.J., Stein, E.A., Yang, Y., 2008. Group independent component analysis reveals consistent resting-state networks across multiple sessions. Brain Res. 1239, 141–151.
Chuang, K.H., van Gelderen, P., Merkle, H., Bodurka, J., Ikonomidou, V.N., Koretsky, A.P., Duyn, J.H., Talagala, S.L., 2008. Mapping resting-state functional connectivity using perfusion MRI. NeuroImage 40, 1595–1605.
Cox, R.W., 1996. AFNI: software for analysis and visualization of functional magnetic resonance neuroimages. Comput. Biomed. Res. 29, 162–173.

Damoiseaux, J.S., Rombouts, S.A., Barkhof, F., Scheltens, P., Stam, C.J., Smith, S.M., Beckmann, C.F., 2006. Consistent resting-state networks across healthy subjects. Proc. Natl. Acad. Sci. U. S. A. 103, 13848–13853.

Davis, T.L., Kwong, K.K., Weisskoff, R.M., Rosen, B.R., 1998. Calibrated functional MRI: mapping the dynamics of oxidative metabolism. Proc. Natl. Acad. Sci. U. S. A. 95, 1834–1839.

De Luca, M., Beckmann, C.F., De Stefano, N., Matthews, P.M., Smith, S.M., 2006. fMRI resting state networks define distinct modes of long-distance interactions in the human brain. NeuroImage 29, 1359–1367.

Desikan, R.S., Ségonne, F., Fischl, B., Quinn, B.T., Dickerson, B.C., Blacker, D., Buckner, R.L., Dale, A.M., Maguire, R.P., Hyman, B.T., Albert, M.S., Killiany, R.J., 2006. An automated labeling system for subdividing the human cerebral cortex on MRI scans into gyral based regions of interest. NeuroImage 31, 968–980.

Di Martino, A., Scheres, A., Margulies, D.S., Kelly, A.M., Uddin, L.Q., Shehzad, Z., Biswal, B., Walters, J.R., Castellanos, F.X., Milham, M.P., 2008. Functional connectivity of human striatum: a resting state FMRI study. Cereb. Cortex 18, 2735–2747.

Donahue, M.J., Blicher, J.U., Østergaard, L., Feinberg, D.A., MacIntosh, B.J., Miller, K.L., Günther, M., Jezzard, P., 2009. Cerebral blood flow, blood volume, and oxygen metabolism dynamics in human visual and motor cortex as measured by whole-brain multi-modal magnetic resonance imaging. J. Cereb. Blood Flow Metab. 29, 1856–1866.

Duong, T.Q., Kim, D.S., Uğurbil, K., Kim, S.G., 2001. Localized cerebral blood flow response at submillimeter columnar resolution. Proc. Natl. Acad. Sci. U. S. A. 98, 10904–10909.

Fernández-Seara, M.A., Wang, Z., Wang, J., Rao, H.Y., Guenther, M., Feinberg, D.A., Detre, J.A., 2005. Continuous arterial spin labeling perfusion measurements using single shot 3D GRASE at 3 T. Magn. Reson. Med. 54, 1241–1247.

Fiser, J., Chiu, C., Weliky, M., 2004. Small modulation of ongoing cortical dynamics by sensory input during natural vision. Nature 431, 573–578.

Fox, M.D., Snyder, A.Z., Vincent, J.L., Corbetta, M., Van Essen, D.C., Raichle, M.E., 2005. The human brain is intrinsically organized into dynamic, anticorrelated functional networks. Proc. Natl. Acad. Sci. U. S. A. 102, 9673–9678.

Greicius, M.D., Krasnow, B., Reiss, A.L., Menon, V., 2003. Functional connectivity in the resting brain: a network analysis of the default mode hypothesis. Proc. Natl. Acad. Sci. U. S. A. 100, 253–258.

Greicius, M.D., Supekar, K., Menon, V., Dougherty, R.F., 2009. Resting-state functional connectivity reflects structural connectivity in the default mode network. Cereb. Cortex 19, 72–78.

Gu, H., Salmeron, B.J., Ross, T.J., Geng, X., Zhan, W., Stein, E.A., Yang, Y., 2010. Mesocorticolimbic circuits are impaired in chronic cocaine users as demonstrated by resting-state functional connectivity. NeuroImage 53, 593–601.

Günther, M., Oshio, K., Feinberg, D.A., 2005. Single-shot 3D imaging techniques improve arterial spin labeling perfusion measurements. Magn. Reson. Med. 54, 491–498.

Hampson, M., Driesen, N.R., Skudlarski, P., Gore, J.C., Constable, R.T., 2006. Brain connectivity related to working memory performance. J. Neurosci. 26, 13338–13343.

Honey, C.J., Sporns, O., Cammoun, L., Gigandet, X., Thiran, J.P., Meuli, R., Hagmann, P., 2009. Predicting human resting-state functional connectivity from structural connectivity. Proc. Natl. Acad. Sci. U. S. A. 106, 2035–2040.

Hua, J., Jones, C.K., Qin, Q., van Zijl, P.C., 2013. Implementation of vascular-space-occupancy MRI at 7 T. Magn. Reson. Med. 69, 1003–1013.

Hudetz, A.G., Biswal, B.B., Shen, H., Lauer, K.K., Kampine, J.P., 1998. Spontaneous fluctuations in cerebral oxygen supply. An introduction. Adv. Exp. Med. Biol. 454, 551–559.

Jin, T., Kim, S.G., 2008. Improved cortical-layer specificity of vascular space occupancy fMRI with slab inversion relative to spin-echo BOLD at 9.4 T. NeuroImage 40, 59–67.

Lu, H., van Zijl, P.C., 2005. Experimental measurement of extravascular parenchymal BOLD effects and tissue oxygen extraction fractions using multi-echo VASO fMRI at 1.5 and 3.0 T. Magn. Reson. Med. 53, 808–816.

Lu, H., Golay, X., Pekar, J.J., Van Zijl, P.C., 2003. Functional magnetic resonance imaging based on changes in vascular space occupancy. Magn. Reson. Med. 50, 263–274.

Lu, H., Clingman, C., Golay, X., van Zijl, P.C., 2004. Determining the longitudinal relaxation time (T1) of blood at 3.0 Tesla. Magn. Reson. Med. 52, 679–682.

Lu, H., Zuo, Y., Gu, H., Waltz, J.A., Zhan, W., Scholl, C.A., Rea, W., Yang, Y., Stein, E.A., 2007. Synchronized delta oscillations correlate with the resting-state functional MRI signal. Proc. Natl. Acad. Sci. U. S. A. 104, 18265–18269.

Menon, V., 2011. Large-scale brain networks and psychopathology: a unifying triple network model. Trends Cogn. Sci. 15, 483–506.

Mohajerani, M.H., McVea, D.A., Fingas, M., Murphy, T.H., 2010. Mirrored bilateral slow-wave cortical activity within local circuits revealed by fast bihemispheric voltage-sensitive dye imaging in anesthetized and awake mice. J. Neurosci. 30, 3745–3751.

Ogawa, S., Lee, T.M., Nayak, A.S., Glynn, P., 1990. Oxygenation-sensitive contrast in magnetic resonance image of rodent brain at high magnetic fields. Magn. Reson. Med. 14, 68–78.

Poser, B.A., Norris, D.G., 2009. 3D single-shot VASO using a Maxwell gradient compensated GRASE sequence. Magn. Reson. Med. 62, 255–262.

Poser, B.A., Norris, D.G., 2011. Application of whole-brain CBV-weighted fMRI to a cognitive stimulation paradigm: robust activation detection in a Stroop task experiment using 3D GRASE VASO. Hum. Brain Mapp. 32, 974–981.

Raichle, M.E., MacLeod, A.M., Snyder, A.Z., Powers, W.J., Gusnard, D.A., Shulman, G.L., 2001. A default mode of brain function. Proc. Natl. Acad. Sci. U. S. A. 98, 676–682.

Smith, S.M., Fox, P.T., Miller, K.L., Glahn, D.C., Fox, P.M., Mackay, C.E., Filippini, N., Watkins, K.E., Toro, R., Laird, A.R., Beckmann, C.F., 2009. Correspondence of the brain's functional architecture during activation and rest. Proc. Natl. Acad. Sci. U. S. A. 106, 13040–13045.

Vidorreta, M., Wang, Z., Rodríguez, I., Pastor, M.A., Detre, J.A., Fernández-Seara, M.A., 2012. Comparison of 2D and 3D single-shot ASL perfusion fMRI sequences. NeuroImage 66C, 662–671.

Viviani, R., Messina, I., Walter, M., 2011. Resting state functional connectivity in perfusion imaging: correlation maps with BOLD connectivity and resting state perfusion. PLoS One 6, e27050.

Wu, W.C., Buxton, R.B., Wong, E.C., 2007. Vascular space occupancy weighted imaging with control of residual blood signal and higher contrast-to-noise ratio. IEEE Trans. Med. Imaging 26, 1319–1327.

Wu, C.W., Gu, H., Zou, Q., Lu, H., Stein, E.A., Yang, Y., 2012. TE-dependent spatial and spectral specificity of functional connectivity. NeuroImage 59, 3075–3084.

Yang, Y., Gu, H., Silbersweig, D.A., Stern, E., 2005. Simultaneous perfusion and blood-oxygenation-level-dependent measurements using single-shot interleaved z-shim echo-planar imaging. Magn. Reson. Med. 53, 1207–1211.

Zou, Q., Wu, C.W., Stein, E.A., Zang, Y., Yang, Y., 2009. Static and dynamic characteristics of cerebral blood flow during the resting state. NeuroImage 48, 515–524.

Zou, Q., Ross, T.J., Gu, H., Geng, X., Zuo, X.N., Hong, L.E., Gao, J.H., Stein, E.A., Zang, Y.F., Yang, Y., 2012. Intrinsic resting-state activity predicts working memory brain activation and behavioral performance. Hum. Brain Mapp.. http://dx.doi.org/10.1002/hbm.22136 [Epub ahead of print, in press].